ELSEVIER

Genetics
in
Medicine

ARTICLE

De Novo *ZMYND8* variants result in an autosomal dominant neurodevelopmental disorder with cardiac malformations

Check for updates

ARTICLE INFO

ABSTRACT

Purpose: *ZMYND8* encodes a multidomain protein that serves as a central interactive hub for coordinating critical roles in transcription regulation, chromatin remodeling, regulation of super-enhancers, DNA damage response and tumor suppression. We delineate a novel neurocognitive disorder caused by variants in the *ZMYND8* gene.
Methods: An international collaboration, exome sequencing, molecular modeling, yeast two-hybrid assays, analysis of available transcriptomic data and a knockdown *Drosophila* model were used to characterize the *ZMYND8* variants.
Results: *ZMYND8* variants were identified in 11 unrelated individuals; 10 occurred de novo and one suspected de novo; 2 were truncating, 9 were missense, of which one was recurrent. The disorder is characterized by intellectual disability with variable cardiovascular, ophthalmologic and minor skeletal anomalies. Missense variants in the PWWP domain of ZMYND8 abolish the interaction with Drebrin and missense variants in the MYND domain disrupt the interaction with GATAD2A. ZMYND8 is broadly expressed across cell types in all brain regions and shows highest expression in the early stages of brain development. Neuronal knockdown of the *Drosophila ZMYND8* ortholog results in decreased habituation learning, consistent with a role in cognitive function.
Conclusion: We present genomic and functional evidence for disruption of *ZMYND8* as a novel etiology of syndromic intellectual disability.

Introduction

Perturbation of highly conserved molecular processes involved in human brain development results in intellectual disability (ID).[1] Despite genetic heterogeneity in ID, many genes converge on interconnected cellular functional networks, such as the regulation of transcription and epigenetic mechanisms.[2]

ZMYND8, also known as *RACK7/PRKCBP1,* encodes a large multidomain protein involved in an extensive protein–protein interaction network. The N-terminal PHD-Bromo-PWWP (PBP) cassette is involved in chromatin-mediated transcription regulation and dual recognition of DNA and histones.[3] Via this cassette, ZMYND8 engages with methylated marks on histone H3 at lysine K4 (H3K4).[3] Alterations to components of the H3K4 machinery have

Kerith-Rae Dias, Colleen M. Carlston, Laura E.R. Blok and Lachlan De Hayr contributed equally.
*Correspondence and requests for materials should be addressed to Tony Roscioli, New South Wales Health Pathology Randwick Genomics, 4th Floor Campus Centre, Barker Street, Randwick, Sydney, New South Wales 2031, Australia. *E-mail address:* tony.roscioli@health.nsw.gov.au
A full list of authors and affiliations appears at the end of the paper.

been implicated in human cognitive dysfunction.[4] The C-terminus contains a leucine zipper (LZ) that enables dimerization of the protein and a myeloid, Nervy, and DEAF-1 (MYND) Zn^{2+} finger domain that regulates ZMYND8 recruitment to sites of DNA damage via chromatin recognition and modification.[5] Functional data have identified ZMYND8 interacting with several complexes involved in transcription regulation.[3,5-7] ZMYND8 interacts directly with Drebrin, which regulates ZMYND8 distribution between the nucleus and synapses.[8] ZMYND8 partners with lysine demethylase 5 (KDM5) family proteins, including KDM5A, KDM5C, and KDM5D to regulate transcription.[6,9] Furthermore, variants in other zinc finger MYND-domain family member genes also result in ID, including *ZMYND5*[10] (also known as *DEAF1*) and *ZMYND11*.[11] In addition, *ZMYND17*[12] and *ZMYND23*[13] have been described as novel candidate genes in ID and *ZMYND22* has been implicated in neurodegenerative disease.[14] Of note, *ZMYND12* is 1 of 3 genes which showed significant upregulation in fibroblasts from individuals with KDM5C-related X-linked ID when compared to controls.[15] A number of MYND-domain family member genes have been implicated in cardiac development and pathology.[16]

Prior to this study, an individual with a de novo variant in *ZMYND8* was reported. A small de novo *ZMYND8* deletion predicted to result in a frameshift was reported by Suzuki et al[17] in an individual with trigonocephaly, speech delay and autism spectrum disorder (ASD) suggesting a role for *ZMYND8* in neurodevelopmental phenotypes. In this study, we assessed clinical data from 10 unpublished individuals combined with newly ascertained information from one affected individual to firmly establish the contribution of *ZMYND8* to ID. In total, 11 individuals had de novo heterozygous *ZMYND8* variants with ID and congenital anomalies, in particular involving the heart. The impact of the variants assessed by ZMYND8 protein–protein interaction assays and a *Drosophila* model with a neurocognitive phenotype provide experimental support for *ZYMND8* as an ID protein hub and a novel cause of Mendelian ID.

Materials and Methods

Cohort recruitment

GeneMatcher[18] and an international collaboration identified a cohort of individuals with *ZMYND8* variants, referred from institutes in the United States, Australia, Ireland, Italy, and Japan. Detailed clinical information was ascertained through the review of medical records. Informed consent for publication was obtained from legal guardians. All parents were unaffected with no family history of ID. Genomic testing was performed as part of routine clinical care.

Clinical sequencing and variant prioritization

ZMYND8 variants were detected by different genomic platforms including exome or genome sequencing using either the Ion Proton System (Thermo Fisher Scientific) or Illumina instrumentation (Supplemental Methods). Bioinformatic pipelines annotated and filtered high-impact variants differing from the reference sequence. Variants were deprioritized if they had tolerant in silico scores, were predicted to have a low impact on protein function, or if they occurred in the Genome Aggregation Database (gnomAD) or internal databases. Variants were reviewed and classified using the American College of Medical Genetics and Genomics and the Association for Molecular Pathology (ACMG/AMP) guidelines.[19] The resulting *ZMYND8* variants, respective to the reference sequence NM_183047.4, were analyzed using a suite of in silico prediction algorithms including Residual Variation Intolerance Score (RVIS), rare exome variant ensemble learner (REVEL), Protein Variation Effect Analyzer (PROVEAN), Combined Annotation Dependent Depletion (CADD), ClinPred, Polymorphism Phenotyping v2 (PolyPhen-2), Sorting Intolerant from Tolerant (SIFT), Functional Analysis Through Hidden Markov Models (FATHMM), Mutation Taster and additional algorithms such as Primate AI. The population frequency of each variant was determined using gnomAD, 1000 genomes and Kaviar. A tolerance landscape for the protein coding regions of *ZMYND8* compared to protein orthologs was generated through MetaDome.[20] Variant interpretations available in ClinVar were assessed.

Molecular modeling

Molecular modeling utilized published structures of the human ZYMND8 PHD-Bromo-PWWP cassette[3,21] (Protein Data Bank [PDB]: 4COS), the PHD-Bromo-PWWP cassette in complex with Drebrin[8,22] (PDB: 5Y1Z) and the LZ and MYND Zn^{2+} finger domain[23] (PDB: 5MQ4). Impacts of missense changes were visualized using Have (y)Our Protein Explained (HOPE) software[24] and Zn^{2+} binding, intra and intermolecular interactions with ChimeraX.[25] ZMYND8 variants were modeled with the swapaa command using the Dunbrack backbone-dependent rotamer library,[26] taking into account the lowest clash score, highest number of H-bonds and highest rotamer probability. Binding of the H3K36me3 peptide was modeled by superimposing the ZMYND11-H3K36me3 structure[27] (PDB: 4N4I) over the ZMYND8 PHD-Bromo-PWWP domain using the matchmaker command in ChimeraX. The binding of histones to ZMYND8 was also modeled.[3,28]

Spatiotemporal analyses of *ZMYND8* expression in the human brain

Expression data from the BrainSpan Atlas was used to examine the expression of *ZMYND8* across brain development.[29]

BrainSpan data consist of reads per kilobase per million mapped reads (RPKM)-normalized values from RNA sequencing data from 8 post conception weeks to 40 years. Ages were binned according to the BrainSpan Technical White Paper. Normalised RPKM expression data were downloaded from BrainSpan and analyzed using R statistical software (v.3.6.2). The regions were classified as either the neocortex or non-neocortex and the expression values were box-plotted using ggplot2 (v3.3.2). The correlation between brain development stage and *ZMYND8* expression values was assessed using a Spearman correlation coefficient using a cor.test() function. In total, 10 fetal and postnatal samples were assessed in each category to account for inter-sample variability and expression across brain regions was assessed using a linear model using lm() and aov() functions. Cell-type specific enrichment analysis of *ZMYND8* was performed using single-cell RNA sequencing adult data across 5 brain regions (hippocampus, dorsolateral prefrontal cortex, subgenual anterior cingulate cortex, nucleus accumbens and amygdala) and the single-cell expression profiles of approximately 40,000 cells were assessed from the developing human neocortex.[30,31] The cell-type specific expression data were log normalized and plotted using the ShinyApp interface and the aggregated cell data through the Cortical Development Expression (CoDeX) viewer.

Protein–protein interaction assays

ZMYND8, Drebrin, and GATAD2A complementary DNAs (cDNAs) were amplified from human brain first-strand cDNA (Takara Bio) using Platinum SuperFi II DNA Polymerase (Thermo Fisher Scientific) and primers listed in Supplemental Table 1. Yeast two-hybrid baits and preys were constructed in pYTH16 and pACT2 vectors[32] using the NEBuilder HiFi DNA Assembly Cloning Kit (New England Biolabs; Supplemental Table 2). Mutant pYTH16-ZMYND8 constructs were made using a novel two-fragment mutagenesis protocol using NEBuilder HiFi DNA assembly, using primers in the origin of replication (ColE1F and ColE1R) and overlapping the desired variant in the *ZMYND8* cDNA (Supplemental Table 1). Protein–protein interaction assays were performed using the yeast strain Y2HGold (Takara Bio). Bait autoactivation was checked by transforming baits with empty pACT2 and 1:10 and 1:100 dilutions and plating on synthetic defined (SD) plates: SD/-Trp, SD/-Trp/X-α-Gal and SD/-Trp/X-α-Gal/Aureobasidin A (AbA). Bait-prey interactions were assessed by plating on SD/-Leu/-Trp double drop-out (DDO) and SD/-Leu/-Trp/X-α-Gal/Aureobasidin A quadruple drop-out (QDO/X/A) plates.

Drosophila Zmynd8 knockdown models

Two *Drosophila* upstream activation sequence-RNA interference (UAS-RNAi) lines targeting non-overlapping regions in the *ZMYND8* ortholog *CG1815* (*Zmynd8* RNAi-1, VDRC107321; *Zmynd8* RNAi-2, VDRC40132) and their respective genetic background controls (VDRC60101 and VDRC 60000) were obtained from the Vienna *Drosophila* Resource Center (VDRC). The line targeting the GATAD2A/B ortholog *simjang* (*simj*) is VDRC100285 (control VDRC60100) and the line targeting the KDM5A-D ortholog lysine demethylase 5 (*Kdm5*) is VDRC42203 (control VDRC 60000). *Drosophila* stocks were maintained at room temperature on standard *Drosophila* diet (sugar, cornmeal, agar and yeast). *Drosophila* genetics and quantitative real-time-PCR analysis are described in Supplemental Methods and Supplemental Table 3.

Drosophila light-off jump reflex habituation and fatigue assays

The habituation and fatigue assays were performed using 3 to 4-day old male flies as described previously[33] and summarized in Supplemental Methods.

Results

Disruption of *ZMYND8* results in syndromic neurocognitive impairment

Phenotypic data were summarized for 11 probands (7 females, 4 males) (Table 1 and Supplemental Table 4). The core clinical features included ID (10/11, 90%) with nonfamilial facial features and cardiovascular anomalies. One individual had profound ID and 2 had moderate ID. Of 11 individuals, 9 had speech delay or language difficulties with 2 exhibiting severe language delay. Nine individuals had motor delay. Congenital cardiac defects were observed in two-thirds of the cohort (7/11, 65%), where at least 5 probands had complex anomalies including patent ductus arteriosus, ventricular septal defect, atrial septal defect, double outlet right ventricle, pulmonary stenosis, right aortic arch, agenesis of the pulmonary artery and patent foramen ovale. Seven individuals (65%) had hearing or vision impairment. Seizures were present in 5 of 11 individuals (45%), including those with the recurrent variant located in the MYND domain. Five individuals had failure to thrive, with slow growth and poor feeding. Four individuals (40%) were diagnosed with ASD and 2 with ASD traits. Four individuals had respiratory tract anomalies including laryngomalacia. The nonfamilial facial features which were present in 80% of the cohort (9/11) were variable, including up-slanting palpebral fissures, hypertelorism, telecanthus, ptosis, upturned nares and thin, sparse, or interrupted eyebrows.

Rare de novo variants are identified in *ZMYND8*

In silico assessment of *ZMYND8* variants are summarized in Supplemental Table 5. Variants were all de novo, absent from population databases, resulted in truncating or missense changes and were located within functional

Table 1 Summary of variant and clinical features of individuals with *ZMYND8* missense and truncating variants

Individual	P1	P2	P3	P4	P5	P6	P7	P8	P9	P10	P11[a]
ZMYND8 variant	p.Gly250Glu	p.Trp311Arg	p.Phe327Leu	p.Lys354Glu	p.Glu954Lys	p.Cys1013Ser	p.His1028Arg	p.Trp1029Arg	p.Trp1029Arg	p.Pro349LeufsTer4	p.Gln822ProfsTer63
Current age and sex	5y, F	3y, F	10y, F	7y, M	NA (deceased at 5 wk), M	7y, F	7y, M	9y, F	F	16y, F	27y, M
De novo	+	+	+	+	+	+	+	+	Suspected	+	+
Affected domain	Bromodomain	PWWP	PWWP	PWWP	Leucine zipper	MYND domain	MYND domain	MYND domain	MYND domain	PWWP	?
Neurobehavioral phenotype (DD/ID/ASD/ speech delay/sleep issues)	+	+	+	+	NA	+	+	+	+	+	+
Cardiovascular anomalies	+	+	+	ND	+	+	ND	+	+	ND	ND
Nonfamilial facial features	+	+	+	+	?	+	+	+	+	ND	+
Minor congenital anomalies (skeletal, brain etc.)	+	ND	+	+	+	ND	+	+	+	+	ND
Vision/hearing impairment	+	ND	+	+	NA	ND	+	+	+	+	ND
Growth (failure to thrive, poor growth, short stature)	+	ND	ND	ND	+	+	ND	ND	+	ND	ND
Seizure	ND	ND	ND	ND	ND	ND	ND	ND	ND	+	+

Variants based on transcript GenBank: RefSeq (NM_183047.4). + indicates present. ? indicates unknown.

ASD, autism spectrum disorder; *DD*, developmental delay; *F*, female; *ID*, intellectual disability; *M*, male; *NA*, not assessed; *ND*, not diagnosed; *P*, proband; *PWWP*, Pro-Trp-Trp-Pro.

[a]Suzuki et al.[17]

domains in regions intolerant to variation. *ZMYND8* is highly evolutionarily constrained and intolerant to variation, ranking in the top 4% of genes intolerant to damaging variation as assessed by RVIS and being extremely intolerant to heterozygous loss of function variants (probability of being loss of function intolerant, pLI = 1). *ZMYND8* is predicted to be intolerant to missense variants with a positive Z-score (Missense Z-score = 4.04) with gnomAD database missense variant depletion. *ZMYND8* has 23 exons, encodes at least 20 protein coding transcripts (Supplemental Table 6), many of which include all known functional domains[5] and is expressed ubiquitously. Fewer than half of these isoforms are expressed across all human tissues with one isoform most likely to be brain-specific (GTex: ENSTO00000311275.11). No other variants were identified in genes relevant to the patient phenotypes.

De novo truncating variants were identified in 2 individuals and 8 de novo and one suspected de novo heterozygous missense variants in 9 individuals, of which one missense variant recurred twice. Two individuals with de novo truncating variants (c.1044delT; p.Pro349LeufsTer4 and c.2465_2469delAGAGG; p.Gln822ProfsTer63) were identified (Table 1 and Supplemental Table 4; Figure 1A). None of the de novo missense variants identified in this cohort have been observed in the gnomAD database. All missense variants were located in regions that are intolerant to variation as assessed by MetaDome (Figure 1B and Supplemental Table 5). The 8 missense variants have CADD scores between 24 and 33 and ClinPred scores between 0.96 and 0.99, consistent with a deleterious impact on gene function. The c.3085T>C; p.Trp1029Arg (p.W1029R) variant is a recurrent variant identified in 2 unrelated probands P8 and P9. The paternal sample for P9 was not available for testing, but as it was not maternally inherited and recurrent in our cohort, its inheritance pattern is suspected to be de novo. All variants were absent in ClinVar and classified as variants of uncertain significance using ACMG/AMP guidelines (Supplemental Table 4).

ZMYND8 is highly expressed in brain development

RNA sequencing data were assessed from 238 fetal and 287 postnatal samples in BrainSpan.[29] *ZMYND8* was highly expressed in the human fetal brain, within the top 30% of expressed genes. *ZMYND8* expression was higher in the prenatal stages, decreased significantly after 25 post conception weeks and remained low postnatally (Supplemental Figure 1), consistent with a role in early brain development. *ZMYND8* showed mild expression variation across brain regions limited to the fetal brain (Supplemental Figure 2). Cell-type specific expression measurements showed that *ZMYND8* is ubiquitously expressed in both neurons and glia in the fetal neocortex[31] and in several regions of the adult human brain[30] (dorsolateral prefrontal cortex, subgenual anterior cingulate cortex, nucleus accumbens and amygdala; Supplemental Figure 3A and B). These data are consistent with a key role for ZMYND8 during brain development.

ZMYND8 variants affect residues critical for binding to Zn^{2+}, histones, DNA and protein interactors

ZMYND8 contains 7 defined structural domains (UniProt Q9ULU4-13; Figure 1A) including monopartite and bipartite nuclear localization sequences (NLS), a PBP cassette comprising a plant homeodomain-type zinc finger (PHD), a bromodomain (Bromo), a second Zn^{2+} finger (ZnF), a Pro-Trp-Trp-Pro motif (PWWP), a putative leucine zipper (LZ) and a myeloid, Nervy, and DEAF-1-type Zn^{2+} finger domain (MYND).[23] Notably, all 8 missense variants are located in known functional ZMYND8 domains or motifs (Figure 1A). Have (y)Our Protein Explained (HOPE) software analysis demonstrated that the *ZMYND8* missense changes result in differences in size, charge or hydrophobicity (Supplemental Figure 4A-H).

PHD-Bromo-PWWP domain variants

Four *ZMYND8* variants are localized within the PBP cassette: p.Gly250Glu (p.G250E) in the bromodomain, and p.Trp311Arg (p.W311R), p.Phe327Leu (p.F327L), and p.Lys354Glu (p.K354E) in the PWWP domain (Figure 1A). The p.G250E variant is located between 2 α-helices, where the substitution of glycine with a glutamic acid, a large, negatively charged residue, is likely to impact on interhelix flexibility. The p.G250E substitution also results in a significant clash with I245 (Supplemental Figure 5A and B). Notably, p.G250E is in close proximity to N248, a key residue for binding to acetylated lysine (Kac site) of histones.[3] The PWWP domain is involved in dual recognition of DNA and methylated histone peptides[3] via an aromatic cage comprising L305, F308, W311, and F327 (Figure 1C). Since missense changes p.W311R and p.F327L affect 2 of these key residues, we superimposed the ZMYND8 PBP cassette over the ZMYND11-H3K36me3 structure to examine this interaction in more detail (Figure 1D-F). We found that W311 and F327 are involved in key cation-π interactions with the trimethyl group of H3K36me3 and that W311 is also involved in a π-π interaction with ZMYND8 residue F359 (Figure 1D). These interactions are predicted to be disrupted by the p.W311R and p.F327L variants (Figure 1D-F), with p.W311R also resulting in clashes with F359 and P309. Taken together, p.G250E, p.W311R, and p.F327L are predicted to interfere with the recognition of histone marks by ZMYND8.

ZMYND8 interactions with Drebrin

The impact of *ZMYND8* PBP cassette variants on the interactions with the neuronal actin-binding protein Drebrin was investigated[8] (Figure 1G-I). ZMYND8 shows Drebrin-dependent synaptic localization,[34] consistent with Drebrin regulating ZMYND8 histone mark recognition by relocating
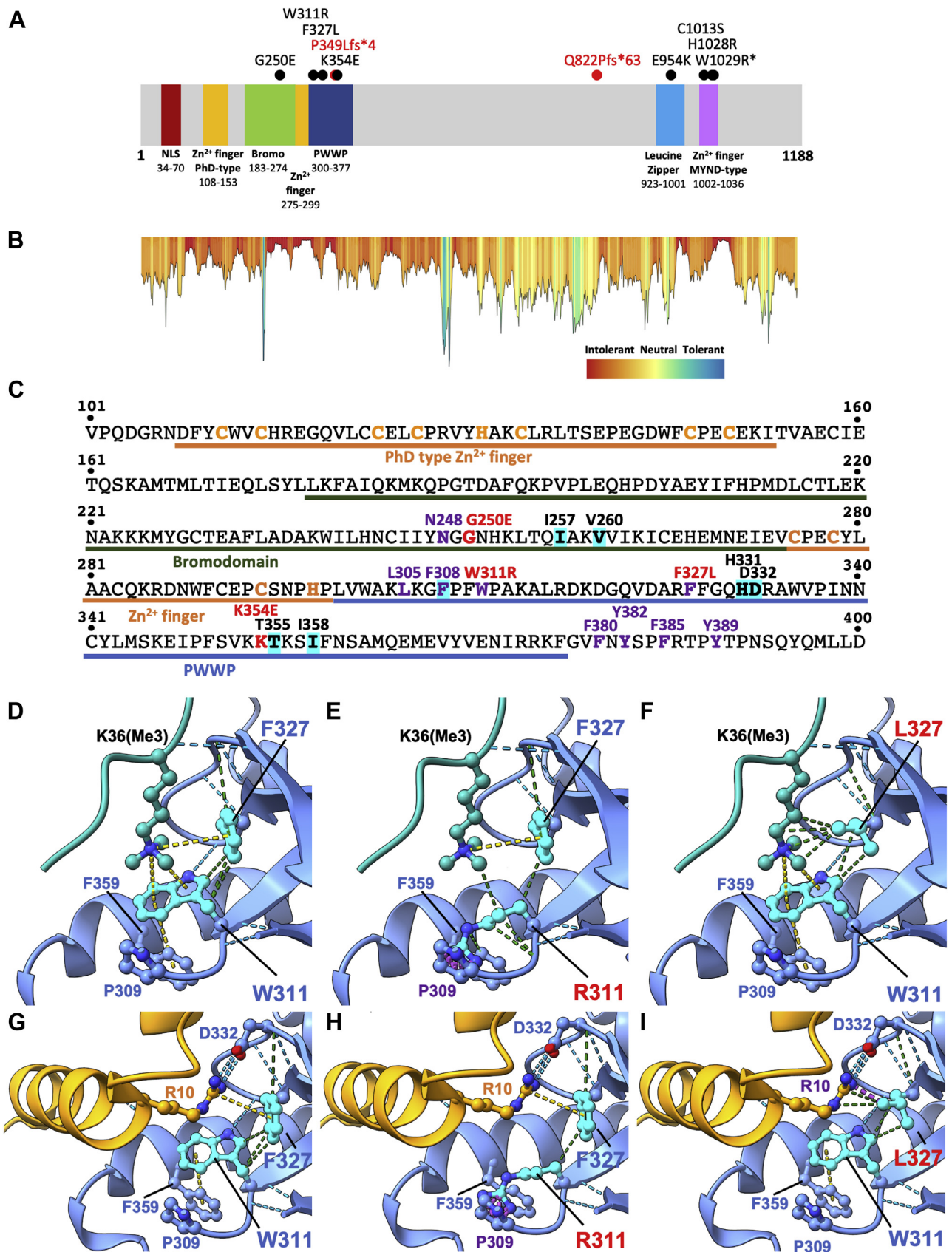
Figure 1 *ZMYND8* **de novo variants in the PHD-Bromo-PWWP (PBP) cassette are predicted to disrupt interactions with histones and Drebrin. A.** Schematic representation of the linear ZMYND8 protein (UniProt Q9ULU4-13; 1188 amino acids) and locations of all variants in the cohort. As indicated, missense variants represented by black circles were identified in 9 individuals and truncating variants

ZMYND8 from nucleus to the cytoplasm.[8] Drebrin interacts with ZMYND8 via an N-terminal actin-depolymerizing factor homology (ADF-H) domain, which in turn binds to 2 sites on the ZMYND8 PBP cassette, involving residues in the Bromo and PWWP domains (Figure 1C). A salt bridge formed by Drebrin R10 with D332 in ZMYND8 is critical for the interaction, and hydrophobic interactions of Drebrin L11, L14, and Y17 with ZMYND8 F308, T355, and I358 also anchor ADF-H to the PWWP site.[8] Binding to the Bromo site is less extensive and involves hydrophobic residues in Drebrin (eg, C96) and ZMYND8 residues I257 and V260.[8] ZMYND8 residue W311 normally makes contacts with F327 (Figure 1G), but the p.W311R substitution disrupts the local structure of this binding pocket through abnormal interactions with P309 and F359 (Figure 1H). The substitution p.F327L also disrupts a cation-π interaction between the side chain of Drebrin R10 with the aromatic ring of F327 (Figure 1G) and results in a clash with Drebrin R10 (Figure 1I).

MYND Zn^{2+} finger domain variants

Variants p.Cys1013Ser (p.C1013S), p.His1028Arg (p.H1028R) and p.W1029R fall within a mutational hotspot in the C-terminal MYND-type Zn^{2+} finger domain (Figure 2A). The MYND domain consists of a cluster of cysteine and histidine residues that form a Zn^{2+}-binding motif. Residues C1002, C1005, C1020, and C1024 coordinate one Zn^{2+}, while C1013, C1014, H1032 and C1036 coordinate another (Figure 2B). Substitution p.C1013S results in the loss of a known Zn^{2+} coordinating residue (Figure 2C and D), predicted to result in a loss of Zn^{2+} binding. Although H1028 is not involved in the direct coordination of Zn^{2+}, the backbone and side chain of this histidine has key contacts with A1003, C1024, Y1019, H1032 and P1030, stabilizing MYND domain folding and orienting a key Zn^{2+} binding residue, H1032. The p.H1028R variant results in the introduction of a larger, positively-charged side chain, resulting in loss of imidazole ring contacts with the Zn^{2+} binding residue H1032 and predicted clashes of the arginine side chain with N1004, Y1019 and Zn^{2+} binding residue C1002. Hence, the p.H1028R variant is also predicted to disrupt Zn^{2+} binding and local folding of the MYND domain (Figure 2E and F). W1029 is also involved in contacts with Zn^{2+} binding residues C1036 and H1032 (Figure 2G and H), contacts lost by p.W1029R, which inserts a larger, positively-charged side chain. Taken together, the p.C1013S, p.H1028R and p.W1029R variants result in disruption of Zn^{2+} binding residues, altered charge, clashes and the loss of key stabilizing contacts with Zn^{2+} binding residues. Notably, the ZMYND8 MYND domain is crucial for regulating ZMYND8 recruitment to sites of DNA damage, via interactions with PPPLΦ motifs in GATAD2A, a key component of the nucleosome remodeling and histone deacetylase (NuRD) multiprotein complex.[5] Hence, disruption of Zn^{2+} binding and/or correct folding of the MYND domain by p.C1013S, p.H1028R and p.W1029R is predicted to disrupt interactions with GATAD2A.

Selected *ZMYND8* missense variants disrupt interactions with Drebrin and GATAD2A

The protein–protein interactions between ZMYND8, the ADF-H domain of Drebrin, and full-length GATAD2A preys were measured in the yeast two-hybrid system. Baits were generated for the ZMYND8 PBP cassette (p.G250E, p.W311R, p.F327L and p.K354E) and LZ-MYND domain (p.C1013S, p.H1028R and p.W1029R) (Figure 3A-B and Supplemental Figure 6). The assays confirmed that p.W311R and p.F327L disrupted ZMYND8-Drebrin interactions, although p.G250E and p.K354E substitutions had no significant effect on this interaction, consistent with the predicted role of K354 in the recognition of histone marks. For the LZ-MYND domain, p.C1013S and p.W1029R, but not p.H1028R, disrupted interactions with GATAD2A (Figure 3B). Further molecular modeling revealed that p.H1028R and p.W1029R change the MYND domain surface structure and/or charge for p.W1029R (Figure 3C-E), but do so at different positions, suggesting

---

represented by red circles in 2 individuals. ZMYND8 consists of 7 major domains: monopartite and bipartite nuclear localization sequences (NLS; 34-70), a PHD-Bromo-PWWP (PBP) cassette comprising a plant homeodomain-type zinc finger (PHD; 108-153), a bromodomain (Bromo; 183-274), a second Zn^{2+} finger (ZnF; 275-299), a Pro-Trp-Trp-Pro motif (PWWP; 300-377) and at the C-terminus, a putative leucine zipper (LZ; 923-1001) and myeloid, Nervy, and DEAF-1-type zinc finger domain (MYND; 1002-1036). Missense variants cluster at the N-terminal end (Bromo, PWWP) and C-terminal end (LZ, MYND). * indicates recurrent variant. **B.** A mutation tolerance landscape along the ZMYND8 protein generated by MetaDome. Genetic tolerance is computed using a missense-over-synonymous ratio over a sliding window of 11 residues based on the variation in gnomAD. Variants located at the N- and C-terminal ends of the ZMYND8 protein correlate with regions of high intolerance to missense changes. **C.** Detailed analysis of key amino acids in the PHD-Bromo-PWWP (PBP) cassette. Positions of *ZMYND8* missense changes are depicted in red type, Zn^{2+} coordinating residues in orange type. Key amino acids for interactions with histones (N248, L305, F308, W311, F327, F380, Y382, F385, Y389) and Drebrin (I257, V260, F308, H331, D332, T355, I358) are indicated by purple lettering and cyan highlighting, respectively. **D-I.** Molecular modeling predicts that missense variants p.W311R, p.F327L and p.K354E disrupt the recognition of histone marks and/or Drebrin. **D-F.** Missense variants p.W311R and p.F327L result in localized clashes disrupting a key cation-π interaction involved in the recognition of the trimethyl group of histone H3. **G-I.** ZMYND8 interactions with Drebrin (orange). Residue W311 normally makes contacts with F327, but the p.W311R substitution results in clashes with P309 and F359, which may disrupt the local structure of this binding pocket for Drebrin. Substitution p.F327L disrupts a cation-π interaction between the side chain of Drebrin R10 with the aromatic ring of F327 and results in a clash with Drebrin R10.
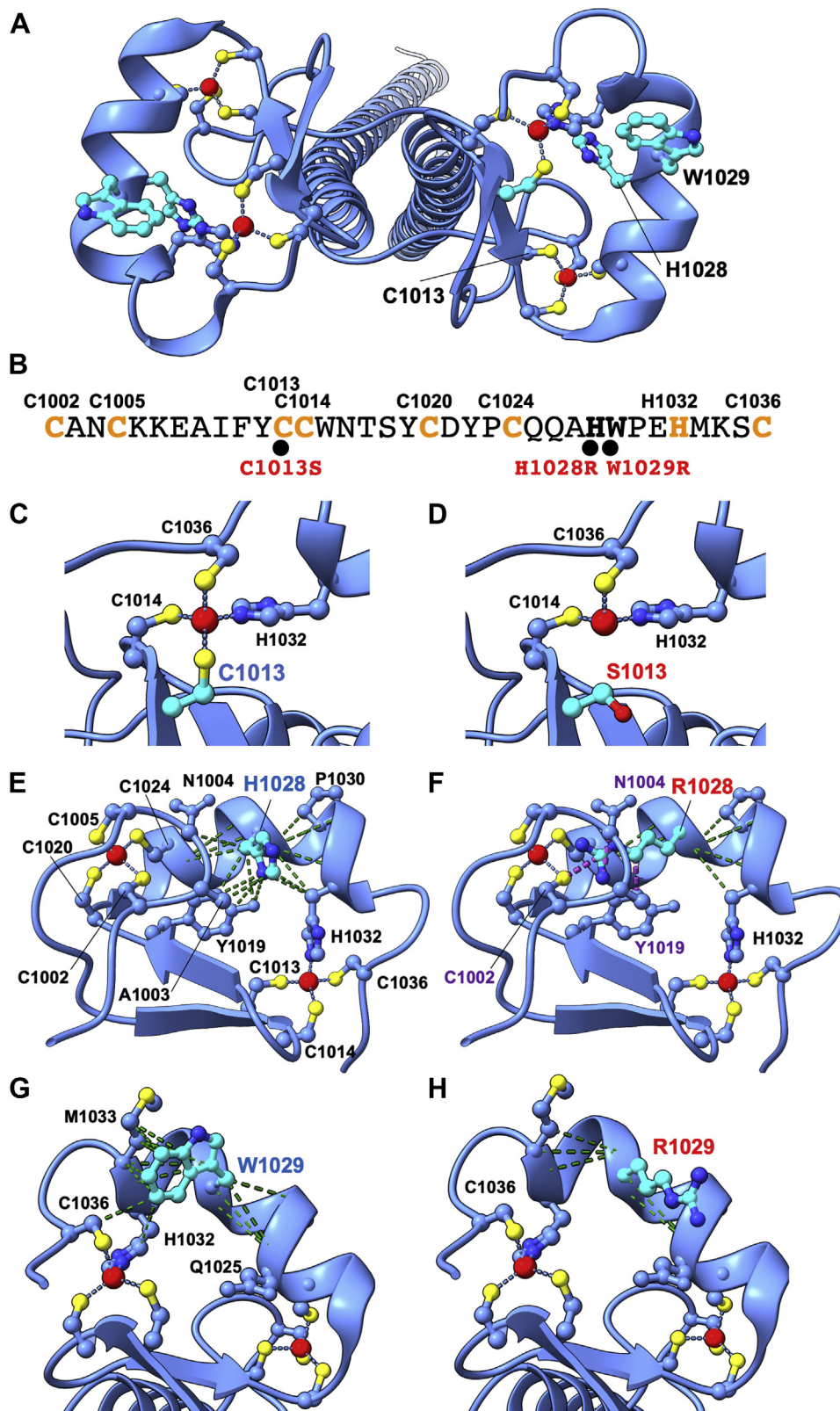
Figure 2   Molecular modeling of *ZMYND8* C-terminal variants. Missense variants p.C1013S, p.H1028R and p.W1029R disrupt Zn^{2+} binding in the MYND Zn^{2+} finger domain. **A, B.** Structure and sequence of the human ZMYND8 MYND domain (PDB: 5MQ4) showing the positions of key residues coordinating Zn^{2+} (red spheres): C1002, C1005, C1020, C1024 coordinate one Zn^{2+}, while C1013, C1014, H1032 and C1036 coordinate a second Zn^{2+}. The positions of residues C1013, H1028 and W1029 are indicated by cyan highlighting of the amino acid side chains in panel A and below the sequence in panel B. **C, D.** The substitution p.C1013S is predicted to result in the loss of a key Zn^{2+} coordinating residue. **E, F.** Although H1028 does not directly coordinate Zn^{2+}, the backbone and side chain of this histidine makes key contacts with A1003, C1024, Y1019, H1032 and P1030, stabilizing the MYND domain and orienting a key Zn^{2+} binding residue, H1032.

that although p.W1029R disrupts ZMYND8-GATAD2A interactions, p.H1028R may disrupt a different MYND domain binding partner. These protein–protein interaction assays validate our bioinformatic and molecular modeling predictions (Supplemental Table 7) and confirm that p.W311R and p.F327L disrupt ZMYND8-Drebrin interactions, while p.C1013S and p.W1029R abolish ZMYND8-GATAD2A interactions, providing evidence of multiple molecular pathomechanisms for *ZMYND8* missense variants.

Neuronal knockdown of *Drosophila Zmynd8* impairs habituation learning

Drosophila harbors a previously uncharacterized one-to-one ortholog of *ZMYND8* (*Zmynd8*, *CG1815*, FBgn003986399). Partial loss of *Zmynd8* function was attempted using the UAS-Gal4 system and 2 lines carrying *Zmynd8*-specific UAS-RNAi constructs (*Zmynd8*-RNAi-1, *Zmynd8*-RNAi-2). First, knockdown efficiency of the 2 constructs was assessed via qPCR upon ubiquitous knockdown with an Actin-GAL4 driver (promoter line). Drivers crossed to the respective genetic background served as a control in all experiments. *Zmynd8*-RNAi-1 significantly knocked *Zmynd8* levels down to 61% ($P = .024$) of control levels (Figure 4A). RNAi-2 showed a tendency but failed to decrease *Zmynd8* levels significantly (88%, $P = .41$) (Supplemental Table 8).

Both lines were crossed to the panneuronal elav-GAL4 driver to target *Drosophila Zmynd8* specifically in neurons and progeny of the appropriate genotype were subjected to the light-off jump habituation paradigm. Habituation is a fundamental, evolutionarily conserved form of non-associative learning that allows organisms to adapt to and filter out meaningless stimuli, a prerequisite for higher cognitive functions. In this assay, control flies (from a cross of the pan-neuronal promotor line and the genetic background line of UAS-*Zmynd8*-RNAi-1) habituated to the light-off stimuli, reducing their jump response over time (Figure 4B, gray). In contrast, pan-neuronal knockdown of *Zmynd8* with UAS-*Zmynd8*-RNAi-1 caused habituation deficits, with *Zmynd8* flies failing to adapt to the levels of their genetic background control (gray) over the entire course of the experiment (Figure 4B, turquoise). Quantification of habituation using the Trials to Criterion score showed a highly significant fold change of 1.7 ($P = 1.78E-10$) for *Zmynd8*-RNAi-1 (Figure 4C), despite the comparatively poor habituation of the genetic background control. With RNAi-2, no effect on habituation was found, most likely because of the poor efficiency of the line (Supplemental Figure 7A-B). Neither of the 2 knockdown

conditions showed motor fatigue as a measure of basal neurologic defects (Supplemental Figure 7C-F). Of interest, we previously identified the fly ortholog of *Zmynd8* interactors KDM5C (*Kdm5*) and GATAD2A/B (*Simj*) to also cause habituation deficits upon pan-neuronal knockdown in the same assay[33] (Supplemental Figure 8A-D). These results are consistent with *Zmynd8* having an important function, specifically in neurons, in habituation learning.
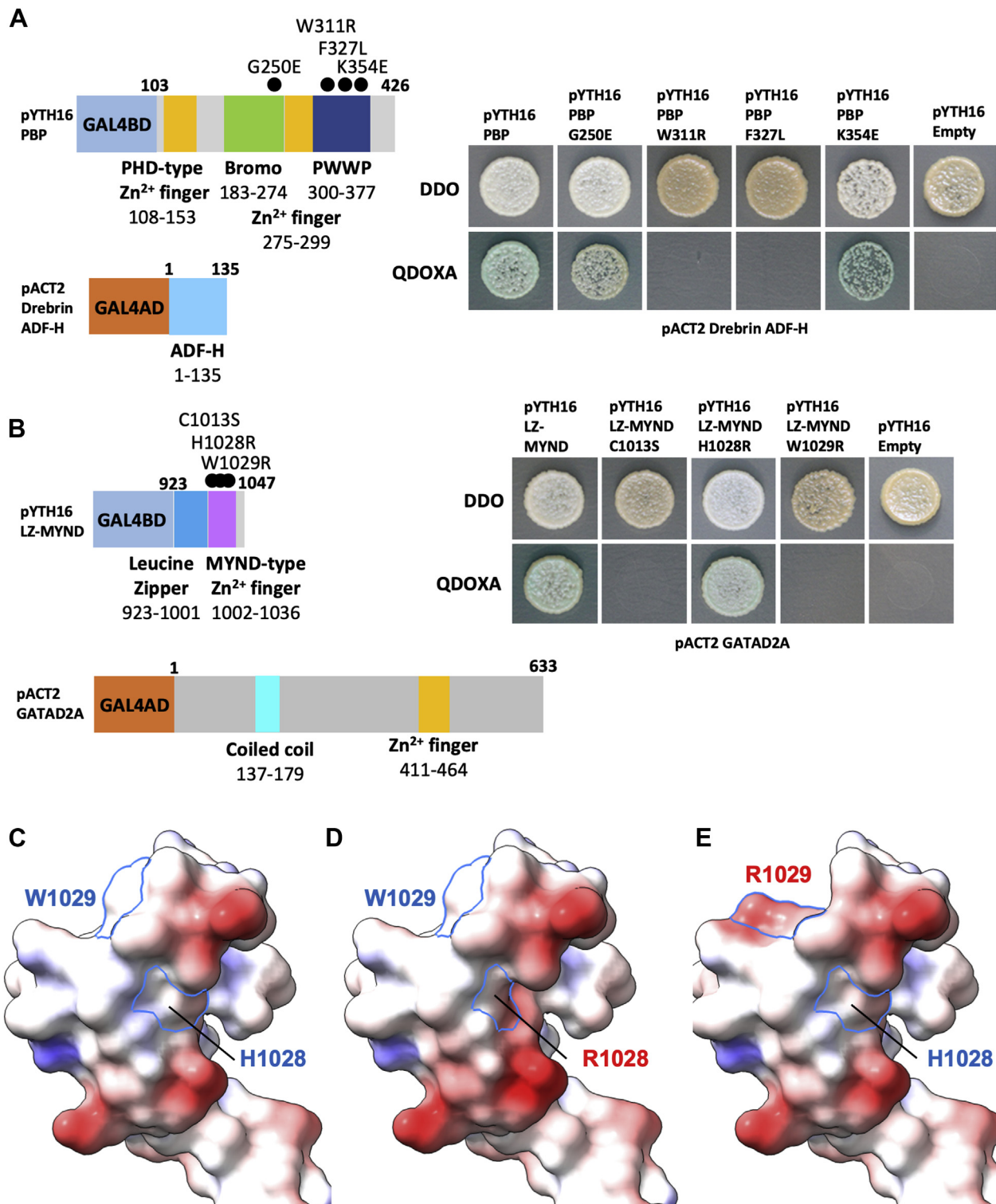
Discussion

Eleven unrelated individuals with a syndromic form of ID including frequent structural cardiac anomalies and associated animal and functional studies provide evidence of the role of *ZMYND8* in ID. All individuals have confirmed or suspected de novo truncating or missense variants in *ZMYND8* that are absent from gnomAD. Molecular modeling and protein–protein interaction assays demonstrated that patient-specific missense variants disrupt interactions of ZMYND8 with Drebrin and GATAD2A. In addition, the functional characterization of neuronal *Zmynd8* knockdown in *Drosophila* models showed deficits in habituation learning, critical for higher cognitive functioning. This evidence establishes de novo variants in *ZMYND8* as a cause of ID with variable congenital anomalies.

Phenotypic variability is expected for large genes with multiple interacting partners, however distinct features were observed within *ZMYND8* mutational hotspots, particularly those involving interacting domains. The 3 individuals with PWWP domain variants had no seizures, mild to moderate developmental delay/intellectual disability (DD/ID) and ASD/ASD traits, whereas the 4 individuals with MYND domain variants had seizures (except p.H1028R), thin or sparse eyebrows, initial slow growth/intrauterine growth restriction, moderate DD/ID and hypotonia. The 2 individuals with the recurrent variant p.W1029R, which disrupts ZMYND8 interaction with GATAD2A, have a strikingly similar phenotype including moderate DD/ID, microcephaly, seizures, hypotonia, cardiovascular and respiratory tract anomalies. Turki et al,[35] reported a de novo variant in *ZMYND8,* known to be expressed in cardiac tissue,[36] in a cohort of individuals with congenital cardiac malformations.

Variants p.G250E and p.K354E do not interfere with Drebrin binding and p.H1028R does not disrupt GATAD2A binding, suggesting that these variants have other pathogenic mechanisms. The individual with p.G250E, has profound cognitive impairment, in comparison to less severe features shared by individuals with other PBP cassette

---

The p.H1028R substitution results in the introduction of a larger positively charged side chain that removes key contacts with H1032 and results in predicted clashes with N1004, Y1019 and C1002. **G, H.** W1029 sits in one of the helices making up the MYND domain and makes contacts with neighboring residues including M1033. The substitution p.W1029R does not create any notable clashes. However, it does lose all significant contacts with M1033.
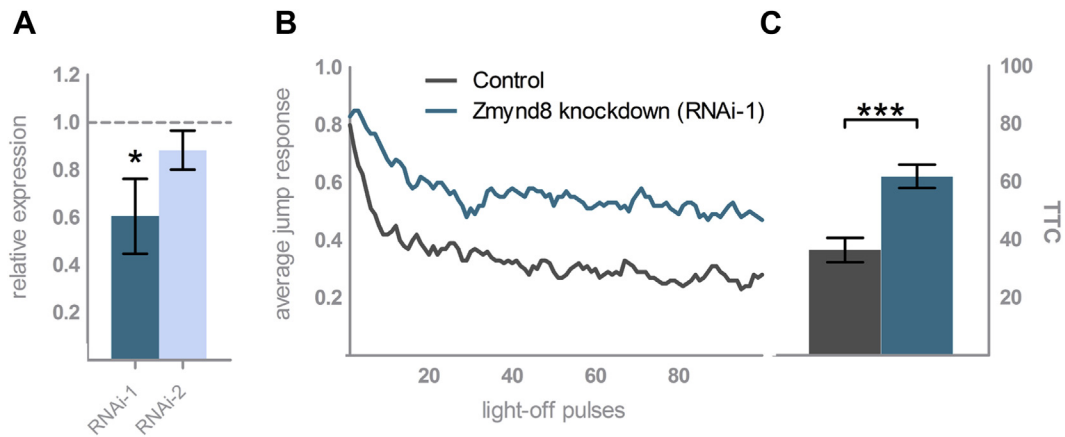
Figure 3 *ZMYND8* **missense variants disrupt interactions with Drebrin and GATAD2A. A.** A yeast two-hybrid (YTH) bait for the ZMYND8 PHD-Bromo-PWWP (PBP) cassette and a prey for the Drebrin actin-depolymerizing factor homology (ADF-H) domain were constructed in vectors pYTH16 and pACT2, respectively. Missense variants G250E, W311R, F327L and K354E were introduced into the PBP cassette bait by site-directed mutagenesis. Bait and prey constructs were transformed into yeast strain Y2HGold and plated onto double drop-out (DDO) and quadruple drop-out (QDO/X/A) plates. Growth on DDO plates demonstrates that both bait and prey vectors were co-transfected, while growth and blue coloration on QDO/X/A plates indicates positive interactions between the wild-type, p.G250E and p.K354E mutants with Drebrin. However, *ZMYND8* missense variants p.W311R and p.F327L clearly disrupt ZMYND8 PBP-Drebrin ADF-H domain interactions. **B.** YTH assays with a ZMYND8 LZ-MYND domain bait and a GATAD2A prey revealed that the wild-type and p.H1028R mutant interact with GATAD2A, while the p.C1013S and p.W1029R missense variants abolish ZMYND8 LZ-MYND domain interactions with GATAD2A. **C-E.** Analysis of the surface impacts of p.H1028R and p.W1029R missense variants indicate that although both variants alter surface charge, they do so at different positions, potentially explaining the differences in impacts on GATAD2A binding. DDO, SD/-Leu/-Trp; QDO/X/A, SD/-Leu/-Trp/X-α-Gal/Aureobasidin A.

Figure 4 *Drosophila Zmynd8* is required, specifically in neurons, for habituation learning. **A.** Relative expression levels of *Zmynd8* mRNA as determined by qPCR upon ubiquitous knockdown induced by *Zmynd8* RNAi-1 and RNAi-2. Error bars indicate standard deviation of three biological replicates. **B.** Pan-neuronal knockdown of *Zmynd8* induced by RNAi-1 (w/Y; 2xGMR-wIR/UAS-RNAi-1; elav-Gal4, UAS-Dicer-2/+, in turquoise) causes slower and incomplete habituation compared to its 40D-UAS genetic background control (w/Y; 2xGMR-wIR/40D-UAS; elav-Gal4, UAS-Dicer-2/+, in gray). **C.** An increase in the mean trials to no jump criterion (mTTC). $N_{\text{40D-UAS control}} = 117$, $N_{\text{RNAi-1}} = 127$, $\text{mTTC}_{\text{40D-UAS control}} = 36.37$, $\text{mTTC}_{\text{RNAi-1}} = 61.81$, $P = 1.78\text{E-}10$. * indicates $P \leq .05$, ** indicates $P \leq .001$, *** indicates $P \leq .0001$. RNAi, RNA interference; TTC, Trials to Criterion.

variants, which could indicate a bromodomain-specific mechanism. Similarly, p.H1028R, which is hypothesized to disrupt a different MYND domain binding partner, has divergent clinical features when compared to the other MYND domain variants that disrupt GATAD2A, including no seizures, MRI anomalies or cardiac defects. The p.E954K variant localizes to the C-terminal LZ, a domain allowing ZMYND8 to form a homodimer associating preferentially with the positive transcription elongation factor b (P-TEFb) complex, required for transcriptional activation of all-trans retinoic acid (ATRA)-mediated differentiation of neuronal precursor cells.[7] The monomer associates with the CHD4 subunit of repressor NuRD complex.[6] Since all *ZMYND8* missense variants are present in the heterozygous state, our functional studies are consistent with a dominant-negative effect, where domain-specific missense variants interfere with specific binding partners.

ZMYND8 is a protein hub interacting with binding partners through different domains (Supplemental Figure 9). De novo missense variants resulting in developmental phenotypes preferentially impact hub proteins within an interactome network enriched for neurodevelopmental disorder genes.[37] ZMYND8 is known to interact with and regulate an increasing number of transcriptional co-repressors, chromatin remodeling complexes, histone demethylase and acetyl transferase enzymes involved in ID (Supplemental Figure 9) consistent with multiple domain-specific mechanisms driving *ZMYND8* ID. Drebrin, a key ZMYND8 interactor, is required to be expressed for normal cognitive development[8] and is a regulator of actin cytoskeleton in neuronal cells, critical for neuritogenesis and neuronal migration.[38] At least 2 *ZMYND8* PBP cassette variants, p.W311R and p.F327L, alter interactions with Drebrin, consistent with

the interference of Drebrin-mediated ZMYND8 localization to synaptic sites[34] (Supplemental Figure 10). Variants p.C1013S and p.W1029R have been shown in this study to disrupt ZMYND8 interactions with the key NuRD complex component, GATAD2A, which recruits ZMYND8 to sites of DNA damage to promote repair by homologous recombination.[5] Deletions in its paralog GATAD2B, also part of NuRD complex, cause a neurodevelopmental disorder (OMIM: 615074).[39] Other NuRD complex members are also implicated in neurodevelopmental disorders with overlapping phenotypes.[40]

Drosophila Zmynd8 knockdown disrupted habituation learning. Habituation deficits have been reported in patients,[41] mouse[42] and more than 100 *Drosophila* models of ID/ASD.[33,43] The diagnosis of co-occurring ASD/ASD traits and ID in 6 individuals in this cohort is thus highly consistent with defective habituation learning observed in the *Zmynd8 Drosophila* model. Moreover, habituation is also disrupted in *Drosophila* models of ZMYND8 interactors in the GATAD2 and KDM5 families. H3K4 methylation is important for human learning and cognition and alterations to its components result in rare neurodevelopmental disorders, such as KMT2A (Wiedemann—Steiner syndrome), KMT2B (dystonia 28), KMT2C (Kleefstra syndrome 2) and KMT2D (Kabuki syndrome 1).[4]

In summary, data presented in this study confirm that de novo heterozygous variants in *ZMYND8* result in a monogenic neurodevelopmental disorder and variable cardiac phenotype. ZMYND8 is a central hub in a conserved network of protein interactions required for habituation learning in *Drosophila* and cognition in humans. In addition to expanding the cohort with detailed genotype–phenotype correlations, the *ZMYND8* syndrome warrants further in-depth variant- and domain-specific studies to define the

contribution of specific variants to the disorder, delineate phenotypic variability and fully represent disease complexity.

Data Availability

This study did not generate datasets or code. All methods are available on request.

Acknowledgments

Author Information

Conceptualization: T.R., C.M.C., K.-R.D.; Data Curation: C.M.C., C.-A.E., P.B.-T., S.H., A.M., S.A.L., C.M., K.S., S.E., M.N.B., J.F., J.G.P., R.R., C.B.N., J.D., T.E.W., M.J.G.S., S.V.M., T.B.P., E.P.K., J.R.P., M.E., F.M., C.G., T.P., B.D., I.G., H.C.M., T.Sh., T.Su., K.Y., H.S., C.P.S., J.C.C., M.F.B., R.J.H.; Formal Analysis: K.-R.D., C.M.C., L.E.R.B., L.D.H., U.N., Y.Z., R.J.H.; Writing-original draft: K.-R.D., L.E.R.B., L.D.H., R.J.H.; Writing-review and editing: T.R., R.J.H., A.S., A.M.S., I.V.

Ethics Declaration

All institutions involved in human participant research received local Institutional Review Board or Research Ethics Committee approval.

This study was approved by the South Eastern Sydney Local Health District Human Research Ethics Committee (main IRB: HREC/13/POWH/203—Gene diagnosis and identification in Mendelian disorders by next-generation sequencing). The individuals included in this study had clinical diagnostic genomic testing with appropriate written consent in their individual hospitals/clinics. Informed consent was obtained from all individuals or was provided by a parent or legal guardian in case of minors or individuals with intellectual disability. Each individual's data, including clinical data are de-identified in accordance with the consent provided by each family.

Web References

University of Washington, Hudson-Alpha Institute for Biotechnology and Berlin Institute of Health. Combined Annotation Dependent Depletion (CADD) Score. Accessed March 9, 2022. http://cadd.gs.washington.edu/

National Center for Biotechnology Information. ClinVar. Accessed March 9, 2022. https://www.ncbi.nlm.nih.gov/clinvar/

Allen Institute for Brain Science. BrainSpan. Accessed March 9, 2022. https://www.brainspan.org/

Allen Institute for Brain Science. BrainSpan Technical White Paper: Transcriptome profiling by RNA sequencing and exon microarray. Published 2013. Accessed March 9, 2022. http://help.brain-map.org/download/attachments/3506181/Transcriptome_Profiling.pdf

Allen Institute for Brain Science. BrainSpan "RNA-Seq Gencode v10 summarise to genes" dataset. Accessed March 9, 2022. https://www.brainspan.org/api/v2/well_known_file_download/267666525

University of Washington. denovo-db. Accessed March 9, 2022. https://denovo-db.gs.washington.edu/denovo-db/

Baylor-Hopkins Center for Mendelian Genomics. Gene-Matcher. Accessed March 9, 2022. https://genematcher.org/

Broad Institute of MIT and Harvard. gnomAD v2.1.1. Accessed March 9, 2022. https://gnomad.broadinstitute.org/

Broad Institute of MIT and Harvard. GTEx Portal Genotype-Tissue Expression Project. Accessed March 9, 2022. https://gtexportal.org/home/

Radboudumc. MetaDome. Accessed March 9, 2022. https://stuart.radboudumc.nl/metadome/

Johns Hopkins University. OMIM. Accessed March 9, 2022. https://www.omim.org/

Protein Data Bank. RCSB PDB. Accessed March 9, 2022. https://www.rcsb.org/

National Center for Biotechnology Information. PubMed. Accessed March 9, 2022. https://pubmed.ncbi.nlm.nih.gov/

National Center for Biotechnology Information. RefSeq: NCBI Reference Sequence Database. Accessed March 9, 2022. https://www.ncbi.nlm.nih.gov/refseq/

Genome Institute. University of California Santa Cruz. UCSC Genome Browser. Accessed March 9, 2022. http://genome.ucsc.edu/

EMBL-EBI. PIR. SIB. UniProtKB. Accessed March 9, 2022. https://www.uniprot.org/

Institute of Genomic Medicine, Wenzhou Medical University & Beijing Institutes of Life Science, Chinese Academy of Sciences. VarCards. Accessed March 9, 2022. http://varcards.biols.ac.cn/

Vienna BioCenter Core Facilities. VDRC. Accessed March 9, 2022. https://stockcenter.vdrc.at/control/main

Conflict of Interest

S.V.M., T.B.P., and M.J.G.S. are employees of GeneDx, Inc. All other authors declare no conflicts of interest.

Additional Information

The online version of this article (https://doi.org/10.1016/j.gim.2022.06.001) contains supplementary material, which is available to authorized users.

Authors

Kerith-Rae Dias[1,2] (iD), Colleen M. Carlston[3], Laura E.R. Blok[4], Lachlan De Hayr[5,6], Urwah Nawaz[7], Carey-Anne Evans[1,8], Pinar Bayrak-Toydemir[9,10], Stephanie Htun[11], Ying Zhu[8], Alan Ma[12,13], Sally Ann Lynch[14], Catherine Moorwood[15], Karen Stals[15], Sian Ellard[15], Matthew N. Bainbridge[16], Jennifer Friedman[16,17], John G. Pappas[18], Rachel Rabin[18], Catherine B. Nowak[19], Jessica Douglas[19], Theodore E. Wilson[20], Maria J. Guillen Sacoto[21], Sureni V. Mullegama[21], Timothy Blake Palculict[21], Edwin P. Kirk[8,22,23], Jason R. Pinner[22,23], Matthew Edwards[24,25], Francesca Montanari[26], Claudio Graziano[26], Tommaso Pippucci[26], Bri Dingmann[27], Ian Glass[27], Heather C. Mefford[28], Takeyoshi Shimoji[29,30], Toshimitsu Suzuki[31], Kazuhiro Yamakawa[31], Haley Streff[32], Christian P. Schaaf[32,33], Anne M. Slavotinek[11], Irina Voineagu[34], John C. Carey[35], Michael F. Buckley[8], Annette Schenck[4], Robert J. Harvey[5,6], Tony Roscioli[1,2,8,23,*] (iD)

Affiliations

[1]Neuroscience Research Australia, Sydney, New South Wales, Australia; [2]Prince of Wales Clinical School, Faculty of Medicine, University of New South Wales, Sydney, New South Wales, Australia; [3]Division of Genetics and Genomics, Boston Children's Hospital, Harvard Medical School, Boston, MA; [4]Department of Human Genetics, Donders Institute for Brain, Cognition and Behaviour, Radboud University Medical Center, Nijmegen, the Netherlands; [5]School of Health and Behavioural Sciences, University of the Sunshine Coast, Maroochydore, Queensland, Australia; [6]Sunshine Coast Health Institute, Birtinya, Queensland, Australia; [7]Adelaide Medical School and Robinson Research Institute, The University of Adelaide, Adelaide, South Australia, Australia; [8]New South Wales Health Pathology, Randwick Genomics Laboratory, Prince of Wales Hospital, Sydney, New South Wales, Australia; [9]Department of Pathology, School of Medicine, University of Utah, Salt Lake City, UT; [10]Molecular Genomics, ARUP Laboratories, University of Utah School of Medicine, University of Utah, Salt Lake City, UT; [11]Division of Medical Genetics, Department of Pediatrics, University of California San Francisco, San Francisco, CA; [12]Department of Clinical Genetics, Children's Hospital Westmead, Sydney Children's Hospitals Network, Sydney, New South Wales, Australia; [13]Specialty of Genomic Medicine, Sydney Medical School, The University of Sydney, Sydney, New South Wales, Australia; [14]Department of Clinical Genetics, Temple Street Children's University Hospital, Dublin, Ireland; [15]Exeter Genomics Laboratory, Royal Devon and Exeter NHS Foundation Trust, Exeter, United Kingdom; [16]Rady Children's Institute of Genomic Medicine, Rady Children's Hospital, San Diego, CA; [17]Departments of Neurosciences and Pediatrics, University of California San Diego, San Diego, CA; [18]Department of Pediatrics, Clinical Genetic Services, NYU Grossman School of Medicine, NYU Langone Health, New York, NY; [19]The Feingold Center for Children, Boston Children's Hospital, Harvard Medical School, Boston, MA; [20]Department of Medical & Molecular Genetics, Indiana University School of Medicine, Riley Hospital for Children at Indiana University Health, Indianapolis, IN; [21]GeneDx, Gaithersburg, MD; [22]School of Women's and Children's Health, University of New South Wales, Sydney, New South Wales, Australia; [23]Centre for Clinical Genetics, Sydney Children's Hospital, Sydney, New South Wales, Australia; [24]Hunter Genetics, Hunter New England Health, New Lambton, New South Wales, Australia; [25]School of Medicine, Western Sydney University, Penrith, New South Wales, Australia; [26]U.O. Genetica Medica, IRCCS Azienda Ospedaliero-Universitaria di Bologna, Bologna, Italy; [27]Medical Genetics Department, Seattle Children's Hospital, Seattle, WA; [28]Center for Pediatric Neurological Disease Research, St. Jude Research, St. Jude Children's Hospital, Memphis, TN; [29]Department of Neurosurgery, Okinawa Pref. Nanbu Medical Center and Children's Medical Center, Okinawa, Japan; [30]Okinawa Central Hospital, Okinawa, Japan; [31]Department of Neurodevelopmental Disorder Genetics, Institute of Brain Sciences, Nagoya City University Graduate School of Medical Sciences, Nagoya, Japan; [32]Department of Molecular and Human Genetics, Baylor College of Medicine, Houston, TX; [33]Institute of Human Genetics, Heidelberg University, Heidelberg University Hospital, Heidelberg, Germany; [34]School of Biotechnology and Biomolecular Sciences, University of New South Wales, Sydney, New South Wales, Australia; [35]Division of Medical Genetics, Department of Pediatrics, University of Utah Health, Salt Lake City, UT

References

1. Vissers LELM, Gilissen C, Veltman JA. Genetic studies in intellectual disability and related disorders. *Nat Rev Genet*. 2016;17(1):9–18. http://doi.org/10.1038/nrg3999

2. Ciptasari U, van Bokhoven H. The phenomenal epigenome in neurodevelopmental disorders. *Hum Mol Genet*. 2020;29(R1):R42–R50. http://doi.org/10.1093/hmg/ddaa175

3. Savitsky P, Krojer T, Fujisawa T, et al. Multivalent histone and DNA engagement by a PHD/BRD/PWWP triple reader cassette recruits ZMYND8 to K14ac-rich chromatin. *Cell Rep*. 2016;17(10):2724–2737. http://doi.org/10.1016/j.celrep.2016.11.014.

4. Collins BE, Greer CB, Coleman BC, Sweatt JD. Histone H3 lysine K4 methylation and its role in learning and memory. *Epigenetics Chromatin*. 2019;12(1):7. http://doi.org/10.1186/s13072-018-0251-8.

5. Spruijt CG, Luijsterburg MS, Menafra R, et al. ZMYND8 co-localizes with NuRD on target genes and regulates poly(ADP-ribose)-dependent recruitment of GATAD2A/NuRD to sites of DNA damage. *Cell Rep*. 2016;17(3):783–798. http://doi.org/10.1016/j.celrep.2016.09.037.

6. Malovannaya A, Lanz RB, Jung SY, et al. Analysis of the human endogenous coregulator complexome. *Cell*. 2011;145(5):787–799. http://doi.org/10.1016/j.cell.2011.05.006.

7. Ghosh K, Tang M, Kumari N, et al. Positive regulation of transcription by human ZMYND8 through its association with P-TEFb complex. *Cell Rep*. 2018;24(8):2141–2154.e6. http://doi.org/10.1016/j.celrep.2018.07.064.

8. Yao N, Li J, Liu H, Wan J, Liu W, Zhang M. The structure of the ZMYND8/drebrin complex suggests a cytoplasmic sequestering mechanism of ZMYND8 by drebrin. *Structure*. 2017;25(11):1657–1666.e3. http://doi.org/10.1016/j.str.2017.08.014.

9. Gong F, Clouaire T, Aguirrebengoa M, Legube G, Miller KM. Histone demethylase KDM5A regulates the ZMYND8-NuRD chromatin remodeler to promote DNA repair. *J Cell Biol*. 2017;216(7):1959–1974. http://doi.org/10.1083/jcb.201611135.

10. Gund C, Powis Z, Alcaraz W, Desai S, Baranano K. Identification of a syndrome comprising microcephaly and intellectual disability but not white matter disease associated with a homozygous c.676C>T p.R226W DEAF1 mutation. *Am J Med Genet*. 2016;170A(5):1330–1332. http://doi.org/10.1002/ajmg.a.37580.

11. Yates TM, Drucker M, Barnicoat A, et al. ZMYND11-related syndromic intellectual disability: 16 patients delineating and expanding the phenotypic spectrum. *Hum Mutat*. 2020;41(5):1042–1050. http://doi.org/10.1002/humu.24001.

12. Riazuddin S, Hussain M, Razzaq A, et al. Exome sequencing of Pakistani consanguineous families identifies 30 novel candidate genes for recessive intellectual disability. *Mol Psychiatry*. 2017;22(11):1604–1614. Published correction appears in *Mol Psychiatry*. 2020;25(11):3101-3102. https://doi.org/10.1038/mp.2016.109.

13. Hu H, Kahrizi K, Musante L, et al. Genetics of intellectual disability in consanguineous families. *Mol Psychiatry*. 2019;24(7):1027–1039. http://doi.org/10.1038/s41380-017-0012-2.

14. Mayfield RD, Zhu L, Smith TA, Tiwari GR, Tucker HO. The SMYD1 and skNAC transcription factors contribute to neurodegenerative diseases. *Brain Behav Immun Health*. 2020;9:100129. http://doi.org/10.1016/j.bbih.2020.100129.

15. Brookes E, Laurent B, Õunap K, et al. Mutations in the intellectual disability gene *KDM5C* reduce protein stability and demethylase activity. *Hum Mol Genet*. 2015;24(10):2861–2872. http://doi.org/10.1093/hmg/ddv046.

16. Rueda-Robles A, Audano M, Álvarez-Mercado AI, Rubio-Tomás T. Functions of SMYD proteins in biological processes: what do we know? An updated review. *Arch Biochem Biophys*. 2021;712:109040. http://doi.org/10.1016/j.abb.2021.109040.

17. Suzuki T, Suzuki T, Raveau M, et al. A recurrent PJA1 variant in trigonocephaly and neurodevelopmental disorders. *Ann Clin Transl Neurol*. 2020;7(7):1117–1131. http://doi.org/10.1002/acn3.51093.

18. Sobreira N, Schiettecatte F, Valle D, Hamosh A. GeneMatcher: A matching tool for connecting investigators with an interest in the same gene. *Hum Mutat*. 2015;36(10):928–930. http://doi.org/10.1002/humu.22844.

19. Richards S, Aziz N, Bale S, et al. Standards and guidelines for the interpretation of sequence variants: a joint consensus recommendation of the American College of Medical Genetics and Genomics and the Association for Molecular Pathology. *Genet Med*. 2015;17(5):405–424. http://doi.org/10.1038/gim.2015.30.

20. Wiel L, Baakman C, Gilissen D, Veltman JA, Vriend G, Gilissen C. MetaDome: pathogenicity analysis of genetic variants through aggregation of homologous human protein domains. *Hum Mutat*. 2019;40(8):1030–1038. http://doi.org/10.1002/humu.23798.

21. Krojer T, Savitsky P, Newman JA, et al. *Crystal structure of the PHD-Bromo-PWWP cassette of human PRKCBP1*. 2018. Accessed March 9, 2022. https://www.rcsb.org/structure/4COS.

22. Yao N, Li J, Liu H, Wan J, Liu W, Zhang M. *Crystal structure of ZMYND8 PHD-BROMO-PWWP tandem in complex with Drebrin ADF-H domain*. 2017. Accessed March 9, 2022. https://www.rcsb.org/structure/5Y1Z.

23. Krojer T, Savitsky P, Picaud S, et al. *Crystal Structure of the leucine zipper of human PRKCBP1*. 2017. Accessed March 9, 2022. https://www.rcsb.org/structure/5MQ4.

24. Venselaar H, Te Beek TA, Kuipers RK, Hekkelman ML, Vriend G. Protein structure analysis of mutations causing inheritable diseases. An e-Science approach with life scientist friendly interfaces. *BMC Bioinformatics*. 2010;11:548. http://doi.org/10.1186/1471-2105-11-548.

25. Pettersen EF, Goddard TD, Huang CC, et al. UCSF ChimeraX: structure visualization for researchers, educators, and developers. *Protein Sci*. 2021;30(1):70–82. http://doi.org/10.1002/pro.3943.

26. Shapovalov MV, Dunbrack RL. A smoothed backbone-dependent rotamer library for proteins derived from adaptive kernel density estimates and regressions. *Structure*. 2011;19(6):844–858. http://doi.org/10.1016/j.str.2011.03.019.

27. Li Y, Ren Y, Li H. *Crystal structure of the Bromo-PWWP of the mouse zinc finger MYND-type containing 11 isoform alpha in complex with histone H3*. 2017:3X36me3. Accessed March 9, 2022. https://www.rcsb.org/structure/4N4G.

28. Qin S, Min J. Structure and function of the nucleosome-binding PWWP domain. *Trends Biochem Sci*. 2014;39(11):536–547. http://doi.org/10.1016/j.tibs.2014.09.001.

29. Kang HJ, Kawasawa YI, Cheng F, et al. Spatio-temporal transcriptome of the human brain. *Nature*. 2011;478(7370):483–489. http://doi.org/10.1038/nature10523.

30. Tran MN, Maynard KR, Spangler A, et al. Single-nucleus transcriptome analysis reveals cell-type-specific molecular signatures across reward circuitry in the human brain. *Neuron*. 2021;109(19):3088–3103.e5. http://doi.org/10.1016/j.neuron.2021.09.001.

31. Polioudakis D, de la Torre-Ubieta L, Langerman J, et al. A single-cell transcriptomic atlas of human neocortical development during midgestation. *Neuron*. 2019;103(5):785–801.e8. http://doi.org/10.1016/j.neuron.2019.06.011.

32. Fuller KJ, Morse MA, White JHM, Dowell SJ, Sims MJ. Development of a yeast trihybrid screen using stable yeast strains and regulated protein expression. *Biotechniques*. 1998;25(1):85–88, 90-92. https://doi.org/10.2144/98251st04.

33. Fenckova M, Blok LER, Asztalos L, et al. Habituation learning is a widely affected mechanism in models of intellectual disability and autism spectrum disorders. *Biol Psychiatry*. 2019;86(4):294–305. http://doi.org/10.1016/j.biopsych.2019.04.029.

34. Yamazaki H, Kojima N, Kato K, et al. Spikar, a novel drebrin-binding protein, regulates the formation and stabilization of dendritic spines. *J Neurochem*. 2014;128(4):507–522. http://doi.org/10.1111/jnc.12486.

35. Al Turki S, Manickaraj AK, Mercer CL, et al. Rare variants in NR2F2 cause congenital heart defects in humans. *Am J Hum Genet*. 2014;94(4):574–585. Published correction appears in *Am J Hum Genet*. 2014;95(1):126. Published correction appears in *Am J Hum Genet*. 2016;98(3):592. https://doi.org/10.1016/j.ajhg.2014.03.007.

36. Fossey SC, Kuroda S, Price JA, Pendleton JK, Freedman BI, Bowden DW. Identification and characterization of PRKCBP1, a candidate RACK-like protein. *Mamm Genome*. 2000;11(10):919–925. http://doi.org/10.1007/s003350010174.

37. Chen S, Fragoza R, Klei L, et al. An interactome perturbation framework prioritizes damaging missense mutations for developmental disorders. *Nat Genet*. 2018;50(7):1032–1040. http://doi.org/10.1038/s41588-018-0130-z.

38. Hanamura K. Drebrin in neuronal migration and axonal growth. In: Shirao T, Sekino Y, eds. *Drebrin: From Structure and Function to Physiological and Pathological Roles*. Springer; 2017:141–155.

39. Shieh C, Jones N, Vanle B, et al. GATAD2B-associated neuro-developmental disorder (GAND): clinical and molecular insights into a NuRD-related disorder. *Genet Med*. 2020;22(5):878–888. Published correction appeared in *Genet Med*. 2020;22(4):822. https://doi.org/10.1038/s41436-019-0747-z.

40. Pierson TM, Otero MG, Grand K, et al. The NuRD complex and macrocephaly associated neurodevelopmental disorders. *Am J Med Genet C Semin Med Genet*. 2019;181(4):548–556. http://doi.org/10.1002/ajmg.c.31752.

41. Ethridge LE, White SP, Mosconi MW, Wang J, Byerly MJ, Sweeney JA. Reduced habituation of auditory evoked potentials indicate cortical hyper-excitability in fragile X syndrome. *Transl Psychiatry*. 2016;6(4):e787. http://doi.org/10.1038/tp.2016.48.

42. Lovelace JW, Wen TH, Reinhard S, et al. Matrix metalloproteinase-9 deletion rescues auditory evoked potential habituation deficit in a mouse model of fragile X syndrome. *Neurobiol Dis*. 2016;89:126–135. http://doi.org/10.1016/j.nbd.2016.02.002.

43. Stessman HAF, Xiong B, Coe BP, et al. Targeted sequencing identifies 91 neurodevelopmental-disorder risk genes with autism and developmental-disability biases. *Nat Genet*. 2017;49(4):515–526. http://doi.org/10.1038/ng.3792.